

Chapter 6: Conditions of ore formation

Abigail Barker

Ore mineral assemblages also record the conditions of ore formation. The most important aspects to the ore geologist are perhaps temperature and oxidation state, however pressure may also be useful to understand the processes of ore formation. The compositions of minerals and mineral assemblages trace the conditions of formation, for which models of thermobarometry and oxygen fugacity have been developed. We will focus on arsenopyrite thermometry, iron-titanium oxide thermometry and indicators of oxygen fugacity and sphalerite thermobarometry.

Goals:

After reading this chapter you should be able to:

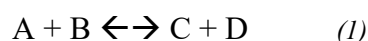
- Describe the theoretical basis of ore mineral thermobarometry.
- Evaluate equilibrium and activity for ore mineral assemblages.
- Explain the application of ore minerals to estimate temperature, pressure and oxygen fugacity.

6.1 Mineral Thermobarometry

Mineral thermobarometers are based on exchange reactions, either resulting from a phase change such as one mineral reacting to form another or substitution and the occurrence of solid solutions, incorporating different cations into the mineral structure. Typically the substituting cations differ from the original cation in for instance ionic radius or even charge and therefore occurs under specific conditions. Geothermometers are commonly based on chemical exchange, whereas geobarometers are typically associated with changes in volume of the mineral structure.

A good geothermometer will be sensitive to temperature, corresponding to a chemical reaction that takes place at a distinct composition and temperature (Fig. 6.01a). In contrast, reactions that occur over a wide temperature range are not temperature sensitive (Fig 6.01b), but may be pressure sensitive, where changing composition relates to a specific pressure (Fig 6.01c).

Mineral thermometers are typically described by an exchange reaction associated with a mineral assemblage that is formed at equilibrium:



At equilibrium there will be no net Gibbs free energy (G), and therefore an equation that describes the thermal properties of the system can be solved:

$$\Delta G = 0 = -RT \ln(K) \quad (2)$$

where R is the gas constant and K is the equilibrium constant, the latter is derived from the activities of the products and reactants:

$$K = \alpha \text{ products (C+D)} / \alpha \text{ reactants (A + B)} \quad (3)$$

Likewise for pressure the equation that governs a reaction is:

$$d\Delta G = 0 = \Delta V dP - \Delta S dT \quad (4)$$

i.e. dP/dT = ΔS/ΔV

where V is the volume and S is the entropy and the terms are derivatives.

Therefore in order to determine the thermobarometric conditions associated with an equilibrium mineral assemblage we need; a) the composition of the minerals that vary, b) a calibrated model for temperature or pressure from experimental data and c) to understand the thermodynamics of the system, such as the activity.

G – Gibbs Free Energy

R – gas constant

K – equilibrium constant

α - change

α - activity

V - volume

S - entropy

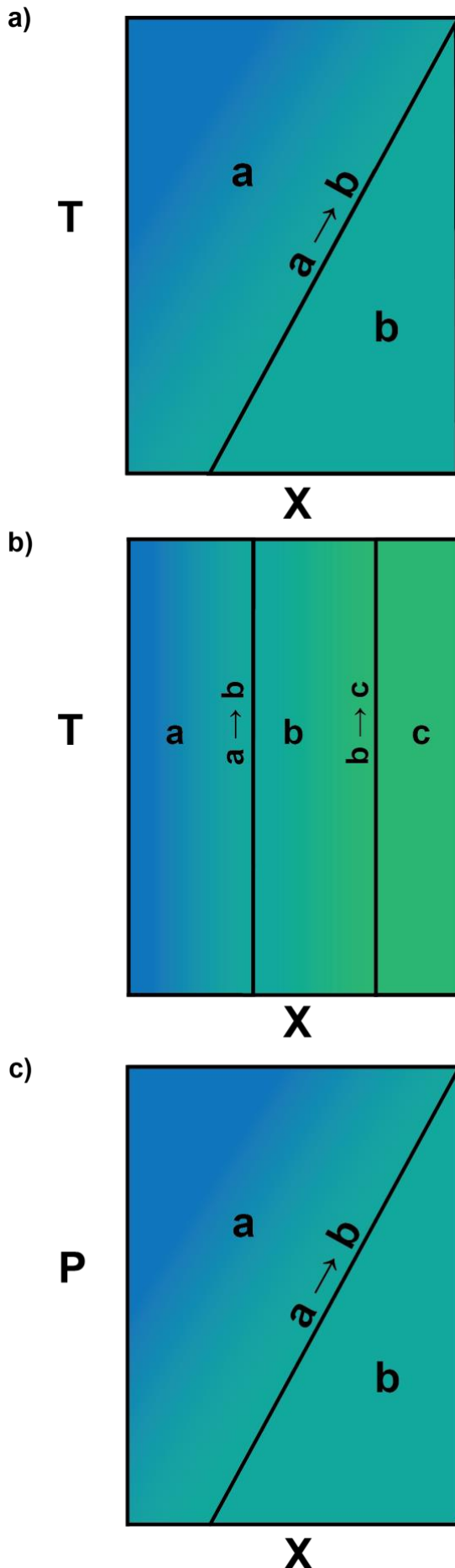


Figure 6.01 Schematic representation of mineral reactions and suitability for thermobarometry.
 a) Temperature (T) versus composition (X), where phase a is stable under different composition and temperature conditions than phase b. The reaction of phase a to phase b occurs with a steep gradient, meaning that the compositional changes reflect specific temperature conditions and thus the reaction is a suitable geothermometer.
 b) The exchange reactions illustrated occur independent of temperature and therefore are not suitable for mineral thermometry.
 c) Pressure (P) versus composition (X) showing that the compositional change, representing a volume change, reflects a pressure change and is therefore a suitable geobarometer.

6.2 Fundamental thermodynamics

Gibbs free energy (G) measures the chemical energy of a system. It is related to the enthalpy or heat content (H), temperature and the entropy or disorder (S) for an individual phase:

$$G = H - TS \quad (5)$$

H – enthalpy (heat content)

S – entropy or disorder

For an exchange reaction such as (1) the difference in Gibbs free energy becomes:

$$\Delta G = \sum G_{\text{products}} - \sum G_{\text{reactants}} \quad (6)$$
$$(G_C + G_D) - (G_A + G_B)$$

Σ - sum

The side of the reaction with the lower Gibbs free energy will be more stable and if the reaction is at equilibrium the energy difference will be neutral ($\Delta G = 0$). Consequently the pressure and temperature conditions are related to ΔG during an exchange reaction at equilibrium. Where the equilibrium constant K is a function of the chemical exchange that describes the chemical or volumetric change. It follows that by constraining the equilibrium constant K, the corresponding pressure and temperature can be determined.

The equilibrium constant (K) relates to the balance in activity of the products and reactants (equation 3). The activity of a pure phase e.g. Fe in FeS₂ will be equal to the mole fraction of Fe, X = 1 and therefore for an ideal solution activity (α) is equal to the composition (X);

*X – composition,
(mole fraction)*

$$\alpha = X \quad (7)$$

or where a cation can occupy several sites (n) the activity is;

$$\alpha = X^n \quad (8)$$

However, most systems show non-ideal behaviour with higher activities associated with disorder and mixing on the cation sites. The higher activities are a function of excess free energy and can be described by Henry's law, with the excess free energy denoted by the activity coefficient (γ), which should be experimentally determined for the system of interest.

γ – activity coefficient

6.3 Arsenopyrite thermometer

In the arsenopyrite structure Arsenic is substituted for Sulphur, and this process is temperature dependent, whereby more As can be incorporated into the mineral structure at higher temperature (Fig. 6.02; Sack & Ebel, 2006). Arsenopyrite is stable up to 702°C. Equilibrium is assessed by the mineral assemblages; a) arsenopyrite + pyrrhotite + löllingite and then in order of increasing temperature; b) arsenopyrite + pyrite, c) arsenopyrite + pyrrhotite and d) arsenopyrite + löllingite (Fig. 6.02).

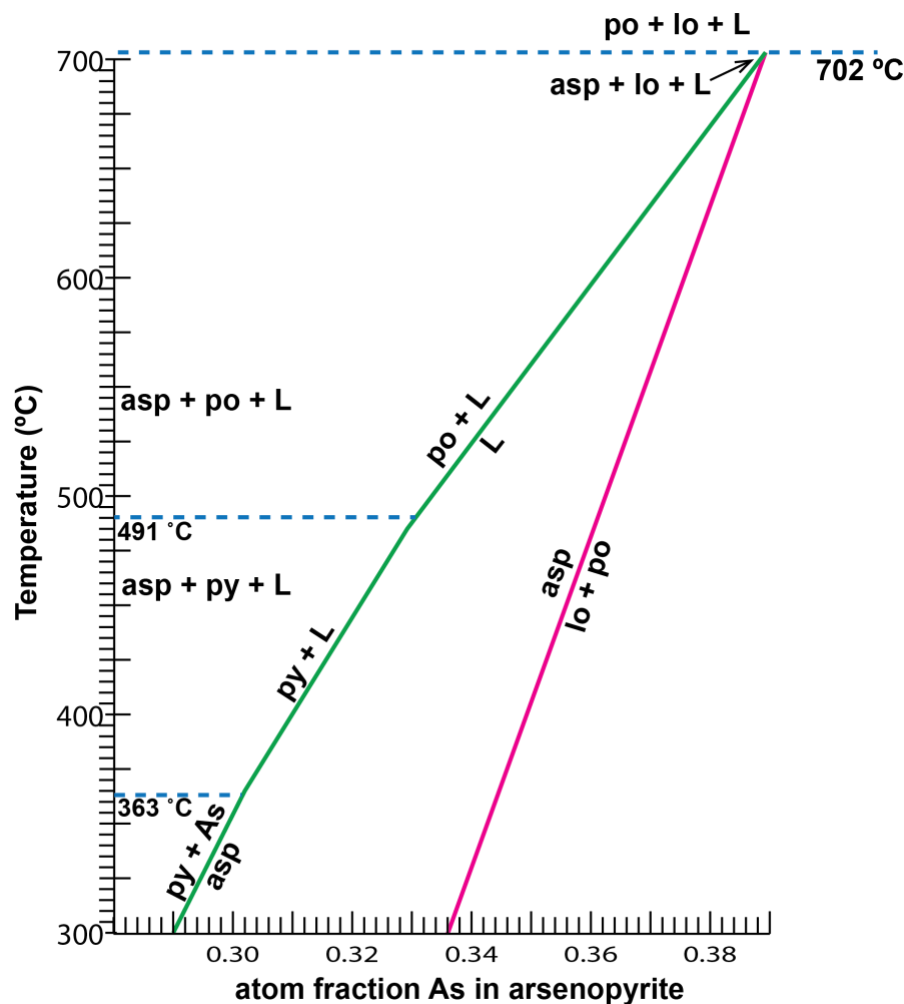


Figure 6.02 Arsenopyrite phase diagram. Arsenopyrite is stable below 702°C. It occurs on reaction of pyrrhotite-löllingite at high As activity and is replaced by pyrrhotite or pyrite at low As activity. The amount of As in arsenopyrite increases with increasing temperature. Modified after Sack & Ebel (2006).

The arsenopyrite thermometer is experimentally constrained and temperatures are determined graphically (Fig 6.03). An example is found at Hornkullen, Bergslagen, Sweden, where arsenopyrite occurs with pyrrhotite, chalcopyrite, galena, pyrite and magnetite. The

arsenopyrite has 33.7 to 36.5 Fe At%, with a mean of 35.4 Fe At% giving an average temperature of 525°C (Andersson, 2014).

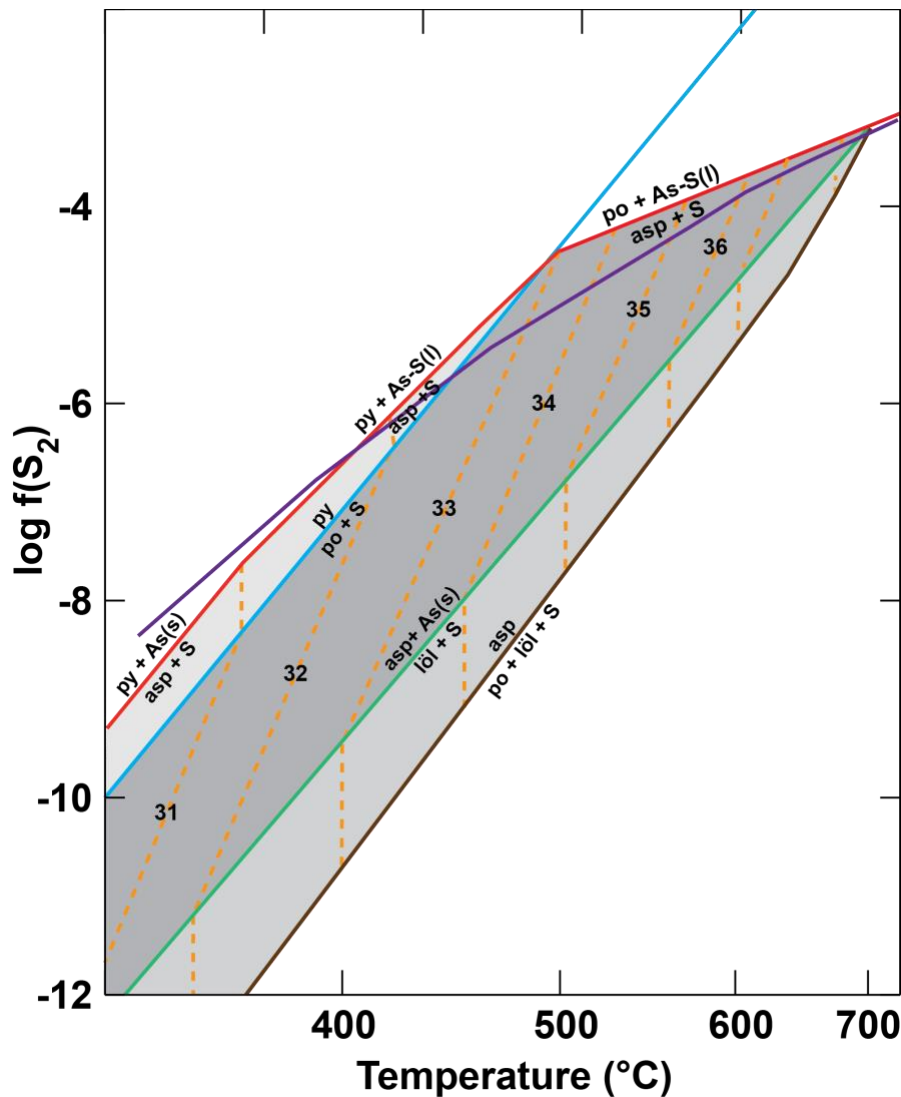


Figure 6.03 Arsenopyrite thermometer. Sulphur fugacity versus temperature. The main mineral assemblages and reactions are shown. The dashed yellow lines depict the As atomic fraction in arsenopyrite, which can be employed to determine the temperature of arsenopyrite formation, after Andersson 2014.

6.4 Magnetite-Ilmenite thermometry

We know from the FeO – Fe₂O₃ – TiO₂ ternary diagram (Fig 2.01), that Fe-Ti-oxides form two solid solutions. One between hematite and ilmenite and a second titanomagnetite solid solution. In addition magnetite and ilmenite can co-exist, with compositional pairs that vary as a function of temperature and oxygen fugacity (Fig 3.08). This section will demonstrate the compositional dependence of ilmenite and magnetite on temperature and implications for mineral growth and re-equilibration.

Firstly we need to consider the activity of the minerals and we will start with magnetite. The magnetite lattice hosts iron cations in both tetrahedral and octahedral sites, which leads us to expect ideal activity approximate to $a = X^2$ (Fig. 6.04a and b). Excess free energy causes the activity to deviate from a model of X^2 . Thus the best expression for the activity of magnetite is derived by including a term for the activity coefficient (γ).

$$a(\text{Fe}_3\text{O}_4) = X^2(\text{Fe}_3\text{O}_4) + \gamma(\text{Fe}_3\text{O}_4) \quad (9)$$

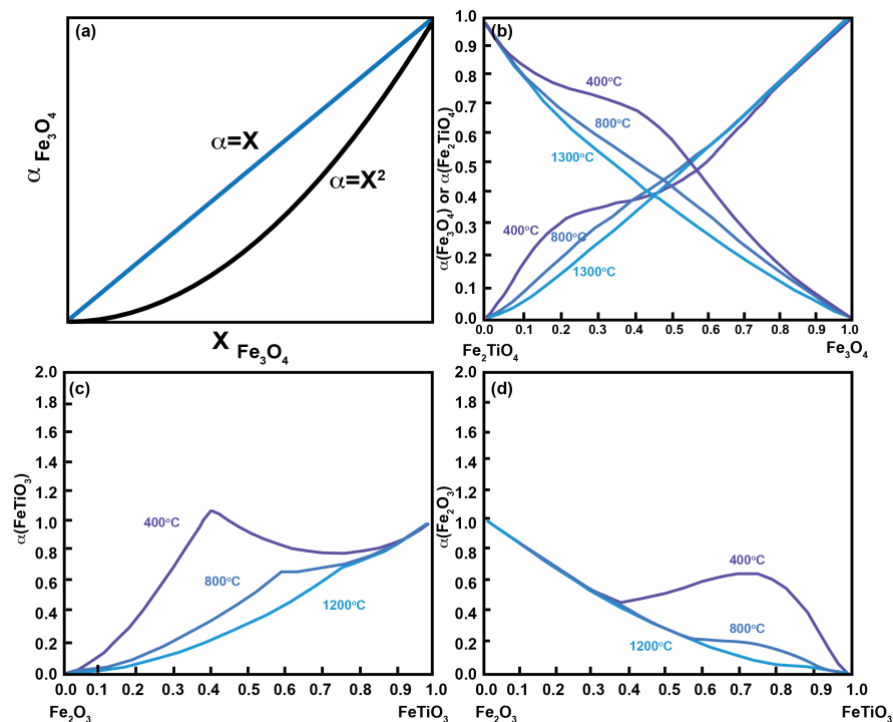


Figure 6.04 Activity for titanomagnetite, hematite and ilmenite. a) magnetite activity with composition showing $a = X$ expected for Fe on one site in the mineral structure and $a = X^2$ as expected for minerals such as magnetite with Fe in two sites of the mineral structure. b) magnetite-ulvöspinel activity-composition relations, showing deviation from ideal $a = X^2$ activity with temperature. c) activity of FeTiO_3 for hematite-ilmenite showing increased activity coefficient a at lower temperatures. d) activity of Fe_2O_3 for hematite-ilmenite showing increased activity coefficient a at lower temperatures. Modified after Ghiorso and Sack (1991).

Instead of modelling magnetite and hematite activities separately Ghiorso and Sack (1991) employ a thermodynamically consistent model of the activities in the iron-titanium oxide system (Fig 6.04b to d). Unlike previous models this does not independently calculate the excess free energy but does predict the miscibility gaps. At temperatures below the Curie point of magnetite (575°C), this method underestimates the excess energy compared to methods using a temperature dependent Margules parameter to provide an activity

co-efficient (γ), which in contrast over estimates the excess free energy at high temperatures above the paramagnetic transition.

Once we have estimated the activities for the system, we can calculate the temperature. Temperature is based on the exchange of Fe and Ti between magnetite and ulvöspinel as well as hematite and ilmenite. In this complex thermodynamic system we use chemical potential (μ) in place of the equilibrium constant and composition, where;

$$\Delta G = \mu(\text{FeTiO}_3) + \mu(\text{Fe}_3\text{O}_4) + \mu(\text{Fe}_2\text{O}_3) + \mu(\text{Fe}_2\text{TiO}_4) \quad (10)$$

The chemical potential is then related to the temperature by an expanded version of the following for each term;

$$\mu(\text{FeTiO}_3) = \mu^\circ\text{FeTiO}_3 \pm \sum RT \ln(x) \pm \sum \Delta G \pm \sum W \quad (11)$$

where W relates to a Margules parameter for the excess free energy.

One question we have not yet considered is the evaluation of equilibrium. For iron oxides, the equilibrium is typically based on observation of co-existing minerals pairs or exsolution textures. An important implication for analyses is therefore to analyse adjacent minerals that are in equilibrium. What process do we constrain the conditions for if we analyse exsolution lamellae?

Visual representations of the compositional temperature relations can be found in Figures 6.05 and 3.09, where the compositions of X_{Usp} and X_{ilm} can be plotted to provide the temperature. Three examples are shown; one with X_{Usp} of 60 and X_{ilm} of 97, giving a temperature of 700°C, a second with X_{Usp} of 50 and X_{ilm} of 92, giving a temperature of 910°C and a third with X_{Usp} of 80 and X_{ilm} of 96, giving a temperature of 950°C.

An example comes from titanomagnetite with ilmenite solid solution features for gneiss in Southeast Norway (Harlov, 2000). Ilmenite dominantly has compositions of X_{ilm} 0.8 to 1.0 and the corresponding magnetite X_{Usp} 0.2 to 0.4, which gives a temperature range of 750 to 850°C.

$$X_{\text{Usp}} = (\text{Ti}/(\text{Ti}+(\text{Fe}^{3+}/2)))*100$$

$$X_{\text{ilm}} = (\text{Fe}^{2+}/(\text{Fe}^{2+}+(\text{Fe}^{3+}/2)))*100$$

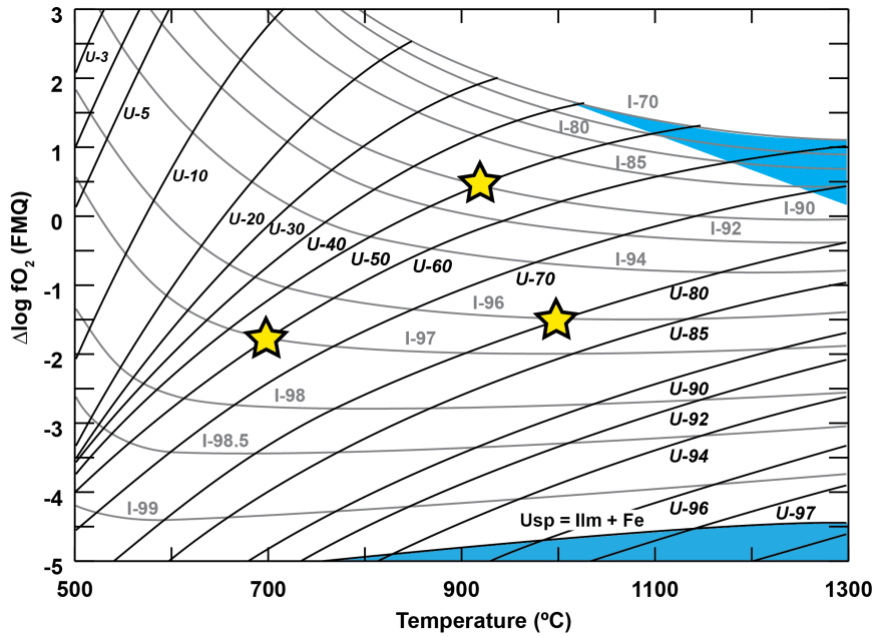


Figure 6.05 Magnetite-Ilmenite thermometry. Oxygen fugacity versus temperature. The grey lines show X_{ilm} and the black lines show X_{usp} . Temperature and oxygen fugacity are determined by the composition of equilibrium magnetite-ilmenite pairs. Stars show three examples, one with $X_{Usp} = 50$, $X_{ilm} = 92$ at 910°C , another at $X_{Usp} = 60$, $X_{ilm} = 97$ and 700°C and a third with $X_{Usp} = 80$, $X_{ilm} = 96$ at 950°C . Modified after Ghiorso and Sack (1991).

6.5 Determination of oxygen fugacity

In an iron-titanium oxide bearing assemblage where the equilibrium temperature is determined, the oxygen fugacity can also be defined by;

$$RT \ln \left(\frac{f_{O_2}}{f_{O_2}^0} \right) = \mu_{O_2} + 6\mu_{Fe_2O_3} - 4\mu_{Fe_3O_4} \quad (12)$$

The oxygen fugacity (f_{O_2}) is either reported as f_{O_2} log units or log units above or below the QFM buffer (Figs. 6.05, 3.09, 2.06; Ghiorso & Sack 1991). For the examples shown in Figure 6.05, the first one with X_{Usp} of 60 and X_{ilm} of 97 has f_{O_2} of -1.7, the second with X_{Usp} of 50 and X_{ilm} of 92 has f_{O_2} of +0.5 and the third example with X_{Usp} of 80 and X_{ilm} of 96 has f_{O_2} of -1.5.

6.6 Sphalerite thermometry

Early attempts at sphalerite thermometry employed the Fe/Zn ratio in sphalerite-pyrrhotite assemblages over the temperature range of 320 to 585°C and required constraint of the sulphur fugacity of the system (Scott and Barnes, 1971). A new approach using global submarine hydrothermal systems as analogues to VMS deposits has

been proposed by Keith et al. (2014). They document a strong negative correlation between Zn (37 to 69 wt%) and Fe (<25 wt%) in sphalerite. Sphalerite that shows chalcopyrite disease, chalcopyrite or pyrite inclusions deviates from this global correlation and are thus easily identified.

Furthermore, the sphalerite samples from sediment-free ridges show a highly positive trend between Fe/Zn and vent fluid temperature (Fig. 6.06; $R^2=0.92$; Keith et al., 2014). This relationship provides a means of calculating the temperature of sphalerite precipitation from the following equation:

$$\text{Fe/Zn}_{\text{sph}} = 0.0013 * T - 0.2953 \quad (13)$$

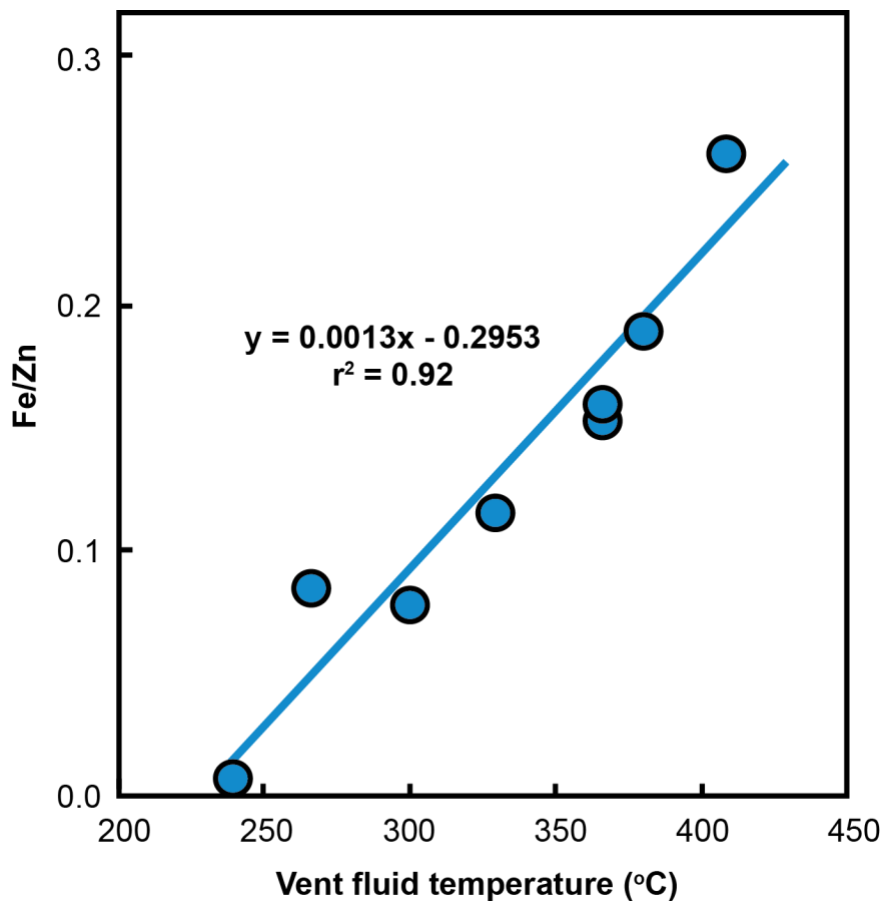


Figure 6.06 The relationship between sphalerite composition and vent fluid temperatures at submarine hydrothermal systems without sediment cover. Modified after Keith et al., (2014).

Initial tests seem promising when samples meet the conditions of sediment-free VMS deposits, no Fe or Cu exchange, no high grade metamorphic overprint and in a temperature range of 220 to 410°C (Keith et al., 2014).

6.7 Sphalerite geobarometry

Sphalerite geobarometry is based on the substitution of Fe for Zn in sphalerite. The phase petrology of the Zn-Fe-S system shows that sphalerite forms a wide solid solution incorporating significant iron, in the presence of both pyrite and pyrrhotite, according to equation 14 (Fig. 6.07).

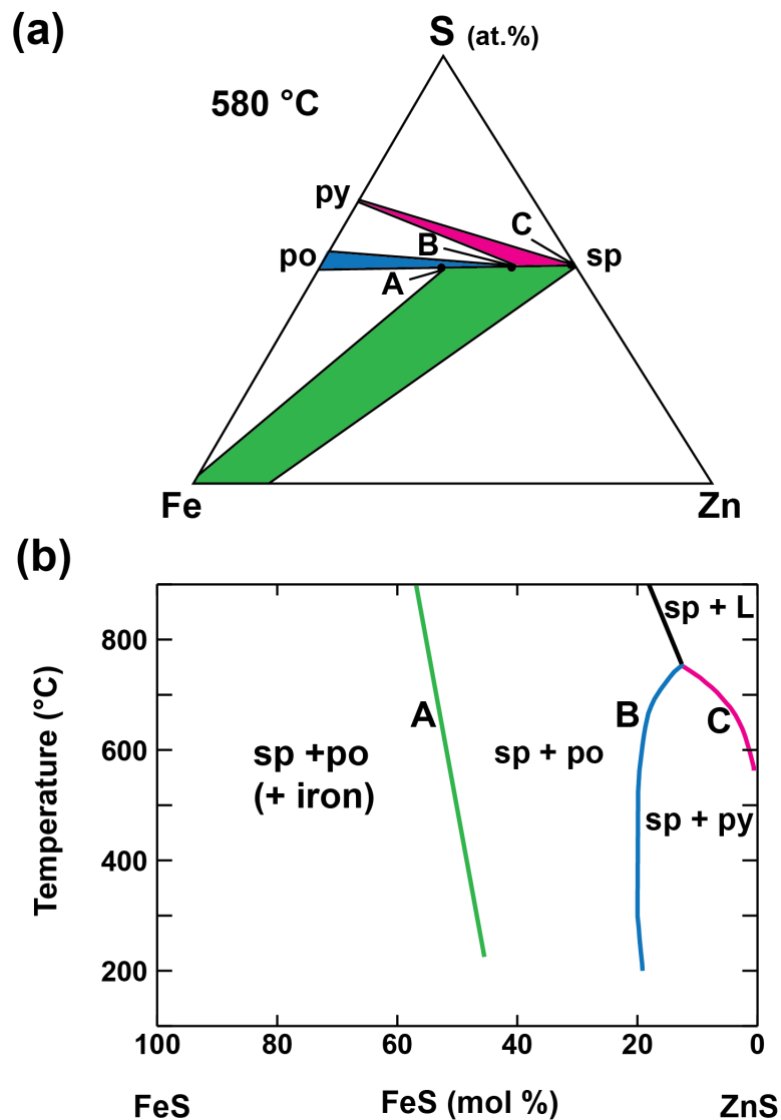


Figure 6.07 Fe-Zn-S phase relations. a) At 580°C pyrite, pyrrhotite and sphalerite are present. The sphalerite composition changes in Fe content between points A and C. b) Temperature versus Fe-Zn-S showing phase assemblages. Modified after Fleet (2006).

An equilibrium assemblage of sphalerite, pyrite and pyrrhotite is required, placing the barometer at the phase boundary B (Fig. 6.07). This phase boundary occurs at approximately 20 mol% FeS over a

wide range of temperature 200 to 700°C at 1 bar, providing evidence that it is not temperature dependent (Fleet, 2006). The iron activity has a far from ideal relationship with the FeS content of sphalerite ($\alpha = X$; only one cation site available), showing significant excess free energy, especially with increasing temperature (Fig. 6.08a). However the activity of Fe in sphalerite is constrained experimentally and generally increases with iron content of sphalerite and pyrrhotite (Fig. 6.09).

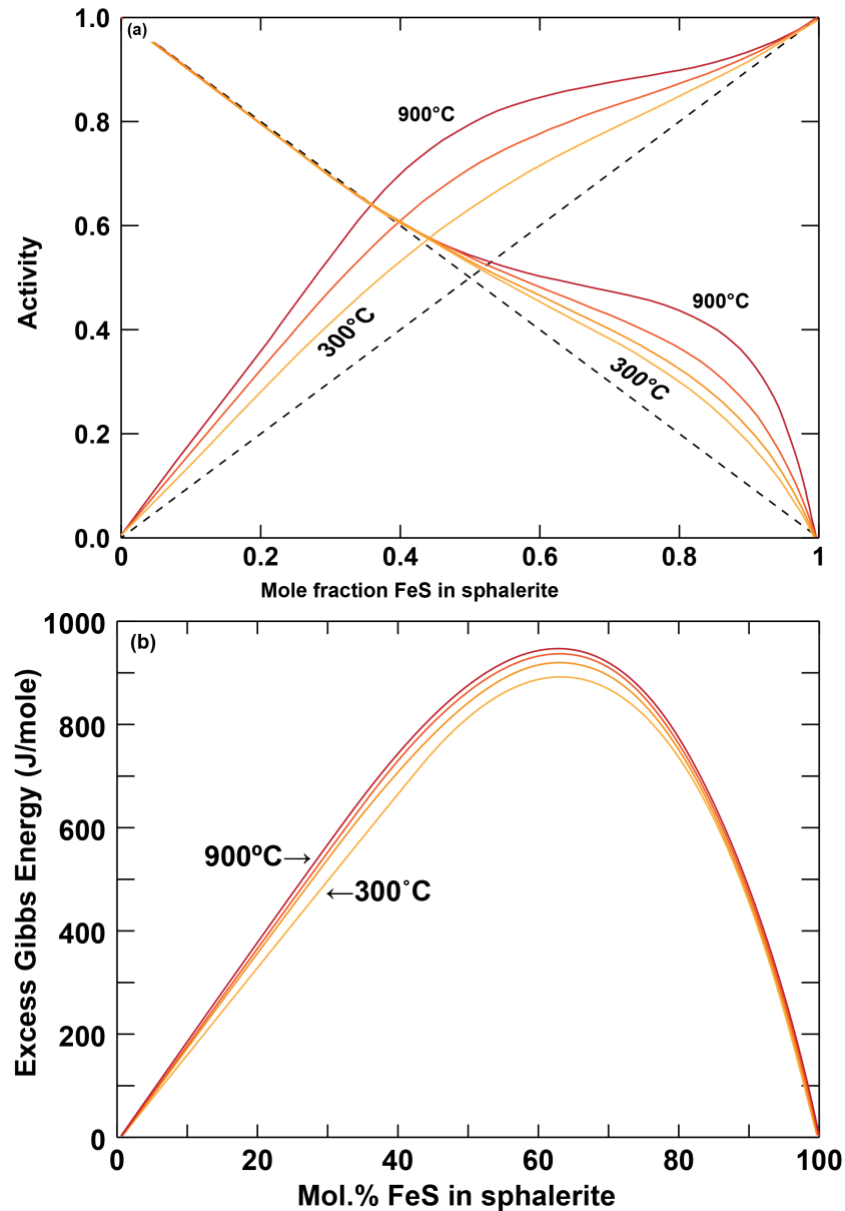


Figure 6.08 Iron activity of sphalerite. a) Activity against FeS content of sphalerite showing the deviation from ideal activity with temperature. b) Excess Gibbs energy against FeS content of sphalerite shows that the maximum excess energy occurs at 60 to 70 FeS mol%, after Fleet (2006).

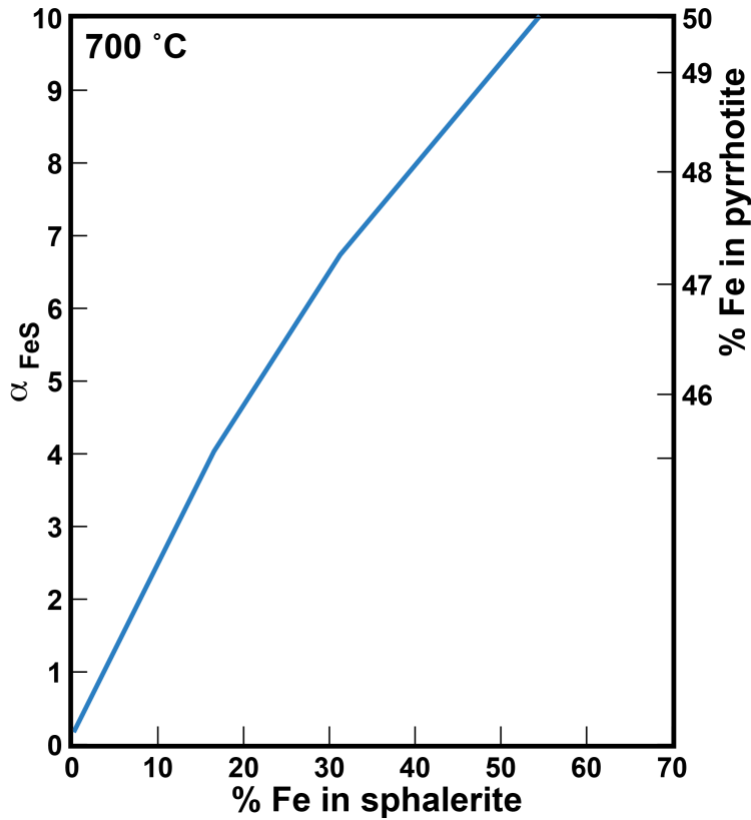


Figure 6.09 FeS activity of sphalerite with composition at 700°C in an assemblage including pyrrhotite. Modified after Fleet (2006).

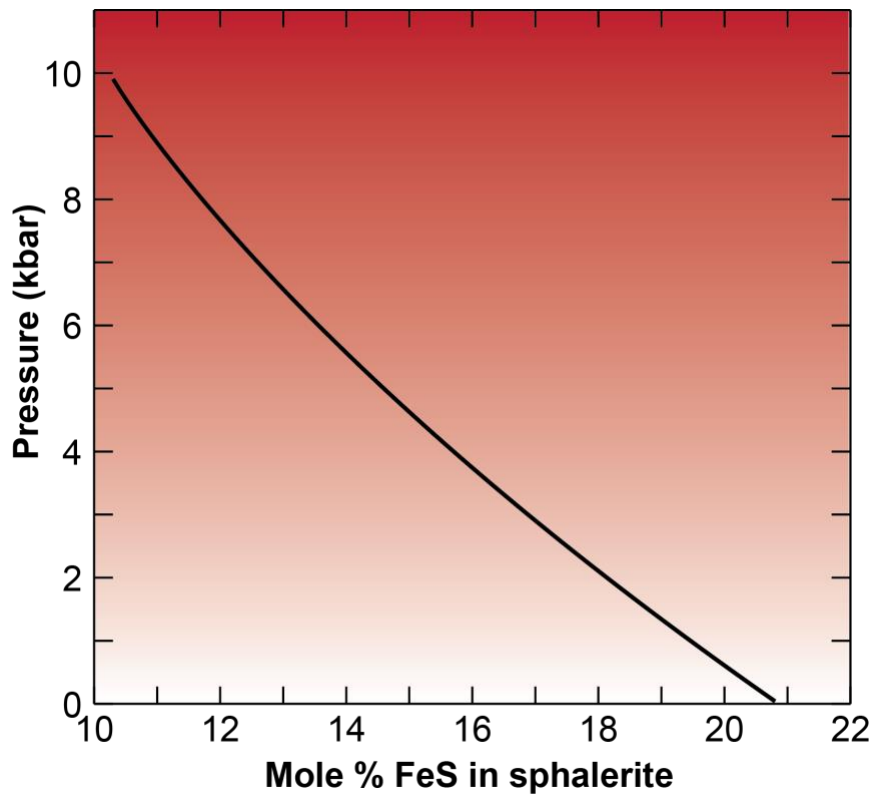


Figure 6.10 Variation of FeS in sphalerite with pressure, after Fleet (2006).

Under equilibrium conditions pressure decreases as more iron is incorporated into sphalerite for a given temperature (Fig. 6.10). Like the arsenopyrite thermometer, the sphalerite barometer is experimentally constrained and pressures are determined by comparison to the isobars for a given composition and temperature (Fig 6.11). Additionally the sphalerite barometer can be described by:

$$\text{FeS}_{\text{sph}} = 20.53 - 1.313P + 0.027P^2 \quad (15)$$

Figure 6.11 shows that a sphalerite composition of 18 FeS mol% corresponds to 2.5 kbar and 10 FeS mol% equates to a pressure of 9.9 kbar (Fleet, 2006).

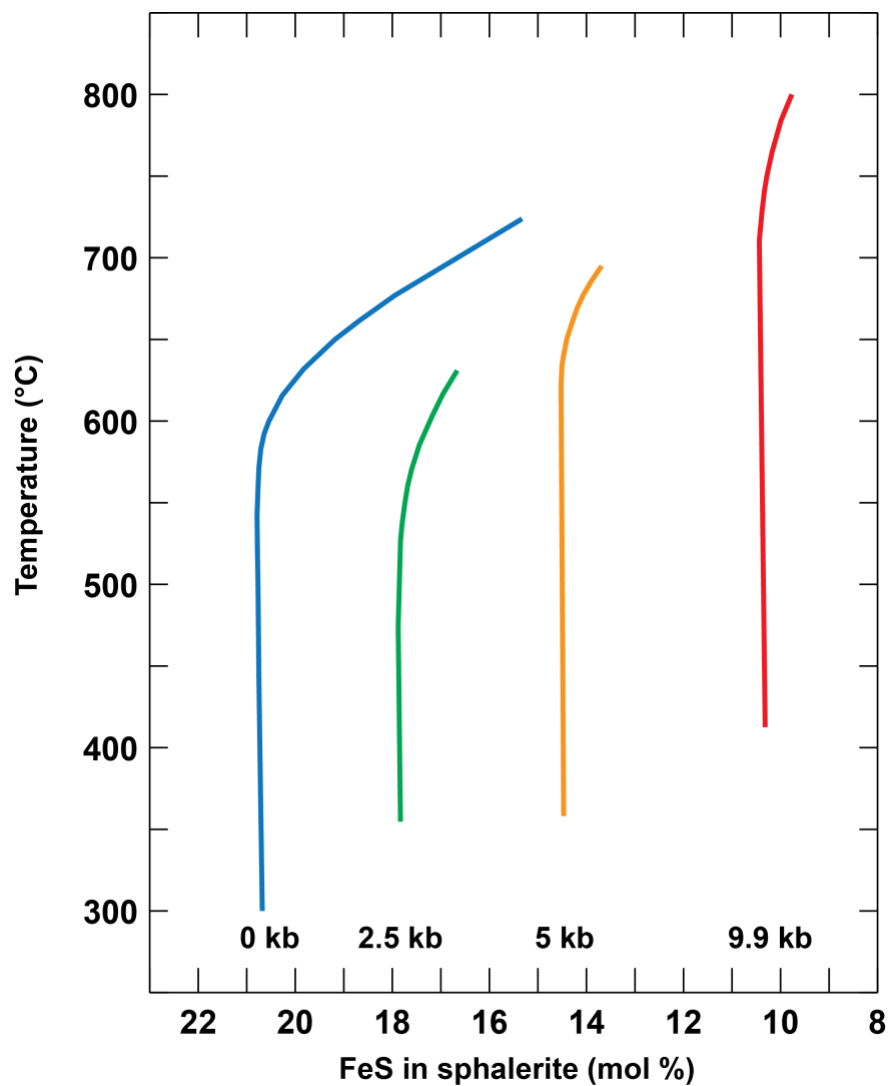


Figure 6.11 Sphalerite geobarometry. Temperature against FeS content of sphalerite. The coloured lines show experimentally determined compositional changes with pressure. Modified after Fleet (2006).

At Hornkullen sphalerite occurs with pyrrhotite, chalcopyrite, galena, pyrite, magnetite and arsenopyrite (Andersson, 2014). The sphalerite has 10 to 15 FeS mol%, therefore the pressure can be estimated to between 5 and 10 kbar.

6.8 Insights from mineral hosted inclusions

Minerals often host mineral, melt and fluid inclusions. The inclusions form or equilibrate at various times during the minerals journey. Melt and fluid inclusions can separate into solid, liquid and gas phases upon cooling, but reheating to the temperature at which they become one phase provides an estimate of their formation temperature. This is known as the homogenisation temperature (T_h). Fluid inclusions may form several populations that can be classified as primary or secondary, based on the textural location of the inclusions in the mineral.

Fluid inclusions also record entrapment or equilibration pressures, which can be assessed from the density of carbon dioxide, analysis by raman spectrometry provides a density dependent raman shift (Ladenberger et al., 2009). The salinity can also be estimated from the density of the fluid, i.e. concentration of NaCl, which can be useful to trace the type of fluids e.g. magmatic, hydrothermal or sedimentary brines, contributing to ore formation (see section 4.1).

The Bingham porphyry ore deposit in Utah, USA is associated with a quartz monzonite, above which potassic alteration (alkali feldspar and biotite) typical of porphyry systems is found (Redmond et al., 2004). Stratigraphically below the ore quartz veins contain CO₂-rich fluid inclusions with salinities of 44 wt% NaCl_{equivalent} and have average T_h of 457°C. Quartz hosted inclusions in the ore zone are also highly saline with 40 wt% NaCl_{equivalent}, but formed at lower temperature T_h of 367°C. The fluid inclusions suggest ascent of ore bearing brines that precipitated chalcopyrite on cooling (Redmond et al., 2004). It is unlikely that meteoric fluids played a significant role due to the high salinities found throughout the alteration halo.

Study Questions

- 1) What inputs are required for a thermobarometric model?
- 2) What is the most suitable expression for magnetite activity? What do the different terms represent?

- 3) What parameters change with temperature for arsenopyrite and magnetite-ilmenite thermometry?
- 4) What equilibrium conditions are required for arsenopyrite and magnetite-ilmenite thermometry and sphalerite geobarometry?
- 5) What temperature corresponds to 33 As mol% in an assemblage of arsenopyrite, pyrrhotite and löllingite?
- 6) What temperature and oxygen fugacity can explain the presence of a) $X_{ilm} 80$ with $X_{usp} 20$ and b) $X_{ilm} 90$ with $X_{usp} 60$? What do you notice about the difference in X_{Ti} between magnetite and ilmenite?
- 7) What pressure is associated with 14.5 FeS mol% in an assemblage of sphalerite, pyrrhotite and pyrite?

Sources and Further reading

Andersson, S. (2014). Deformation, metamorphism and remobilisation in the Hornkullen polymetallic deposit, western Bergslagen, Sweden. Examensarbete vid Institutionen för geovetenskap, ISSN 1650-6553; 284. [urn:nbn:se:uu:diva-223246](https://nbn-resolving.org/urn:nbn:se:uu:diva-223246)

Fleet, M.E., (2006) Phase Equilibria at High Temperatures In: Editor Vaughan, D.J., Sulfide mineralogy and geochemistry MSA Reviews in Mineralogy Volume 61, p 365-420, ISBN 0-939950- 73-1

Ghiorso, M.S., and Sack, R.O., (1991). Fe-Ti oxide geothermometry: thermodynamic formulation and the estimation of intensive variables in silicic magmas. *Contrib Mineral Petrol* 108: 485-510.

Harlov, D.E., (2000). Titaniferous magnetite±ilmenite thermometry and titaniferous magnetite±ilmenite ±orthopyroxene±quartz oxygen barometry^[1] in granulite facies gneisses, Bamble Sector, SE Norway: implications for the role of high-grade CO₂-rich fluids during granulite genesis. *Contrib Mineral Petrol* 1139: 180-197.

Keith, M., Haase, K.M., Schwarz-Schampera, U., Klemm, R., Petersen, S., Bach, W., (2014). Effects of temperature, sulphur, and oxygen fugacity on the composition of sphalerite from submarine hydrothermal vents. *Geology* 42(8), 699-702. doi:10.113/G35655.1

Ladenberger, A., Lazor, P., & Michalik, M. (2009). CO₂ fluid inclusions in mantle xenoliths from Lower Silesia (SW Poland): formation conditions and decompression history. *European journal of mineralogy*, 21(4), 751-761.

Philpott, A.R., and Ague, J.J., (2009). Principles of Igneous and Metamorphic Petrology. Cambridge University Press ISBN 9780521880060

Sack, R.O., and Ebel, D.S., (2006). Thermochemistry of Sulfide Mineral Solutions In: Editor Vaughan, D.J., Sulfide mineralogy and geochemistry MSA Reviews in Mineralogy Volume 61, p 365, 420, ISBN 0---939950---73---1

Scott, S.D., Barnes, H.L. (1971). Sphalerite geothermometry and geobarometry: Economic Geology and the Bulletin of the Society of Economic Geologists 66, 653-669.
doi:10.2113/gsecongeo.66.4.653.

Redmond, P.B., Einaudi, M.T., Inan, E.E., Landtwing, M.R., Heinrich, C.A. (2004). Copper deposition by fluid cooling in intrusion-centered systems: New insights from the Bingham porphyry ore deposit, Utah. *Geology* 32(3), 217-220.
Doi:10.113/G19986.1

White, W.M., (2013) Applications of thermodynamics to the Earth In: Geochemistry John Wiley and Sons ISBN 978-0470656686.